International Journal of Heat and Mass Transfer 96 (2016) 371–380

Contents lists available at ScienceDirect

International Journal of Heat and Mass Transfer

journal homepage: www.elsevier.com/locate/ijhmt

An improved transient plane source method for measuring thermal conductivity of thin films: Deconvoluting thermal contact resistance

Mohammad Ahadi [a], Mehdi Andisheh-Tadbir [a], Mickey Tam [b], Majid Bahrami [a,*]

[a] Laboratory for Alternative Energy Conversion (LAEC), School of Mechatronic Systems Engineering, Simon Fraser University, Surrey, BC V3T 0A3, Canada
[b] Structure, Properties & Performance Research Division, Automotive Fuel Cell Cooperation Corp. (AFCC), 9000 Glenlyon Parkway, Burnaby, BC V5J 5J8, Canada

ARTICLE INFO

Article history:
Received 11 November 2015
Received in revised form 1 January 2016
Accepted 13 January 2016
Available online 4 February 2016

Keywords:
Thermal conductivity
Thin film
Transient plane source (TPS) method
Thermal contact resistance (TCR)
Hot disk thermal constants analyzer
Guarded hot plate method

ABSTRACT

The conventional transient plane source (TPS) method cannot accurately measure bulk thermal conductivity of thin films and coatings, because of the inclusion of thermal contact resistances in the results. In this study, a new modified TPS method is proposed that allows accurate measurement of bulk thermal conductivity of thin films and coatings. For this purpose, first, a hot disk testbed is used to measure the total thermal resistance for different thicknesses of a sample in the TPS test column. The bulk thermal conductivity is then deconvoluted from the results. Experiments have been performed on ethylene tetrafluoroethylene (ETFE) sheets, Nafion membranes, and gas diffusion layers (GDLs) with different thicknesses using the proposed method, and the results have been cross-checked with the data obtained from the guarded hot plate method, as per ASTM standard C177-13. The present modified TPS method yields thermal conductivity values of $0.174 \pm 0.002\ W{\cdot}m^{-1}{\cdot}K^{-1}$ for ETFE and $0.243 \pm 0.007\ W{\cdot}m^{-1}{\cdot}K^{-1}$ for Nafion, while the values measured by the guarded hot plate method are $0.177 \pm 0.002\ W{\cdot}m^{-1}{\cdot}K^{-1}$ for ETFE and $0.214 \pm 0.003\ W{\cdot}m^{-1}{\cdot}K^{-1}$ for Nafion. The GDL results, on the other hand, change with mechanical pressure, and about 15.7% difference is observed between the GDL results of the two methods. Overall, the developed method is proved to be highly reliable, quick, and accurate.

1. Introduction

Thermal management is crucial in increasingly small areas like thin gas diffusion layers and catalyst layers [1–5], microelectronic packages and microprocessors [6–8], and ink coatings [9]. Precise thermal conductivity measurement is one of the key parameters needed in such applications. Thermal properties measurement methods can be classified as: (i) steady state and (ii) transient [10–25]. The steady-state methods have the advantage of simplicity of the analysis of the signal and the main disadvantage of long measurement times, whereas transient thermal properties tests are much quicker and more complex to analyze. As the focus of this study is on transient methods, a brief review of the features of the available transient methods is provided in Table 1. More information on steady-state methods can be found elsewhere [10,11].

In this study, transient plane source (TPS) experiments were performed with a sensor of thin double spiral nickel sandwiched between two thin "Kapton" films providing the sensor with electrical insulation and mechanical stability; the sensor acts as a plane heat source and a resistance thermometer, see Fig. 1. The thermal transport properties of a sample can be obtained from analysis of temperature increase of the sensor registered by the sensor, itself, as a function of time. Details of the analytical solution of a transient heat source on a half-space, i.e., the fundamental of TPS method, can be found in [16–19] and are briefly explained in the next section of this article.

In the hot disk technology, an effective thermal conductivity is measured for a thin film, which contains: (i) the bulk thermal resistance of the film, (ii) the thermal contact resistance (TCR) between the film and the TPS sensor, (iii) the TCR between the film and the background material, (iv) the TCR between the adhesive sticking the Kapton layer of the TPS sensor to its double spiral nickel and the double spiral nickel, and (v) the TCR between the TPS sensor and the background material associated with the required reference tests according to ISO22007-2 [18]. As such, the measured value of bulk thermal conductivity is not accurate and contains the mentioned TCRs. In the present study, the current TPS method for thin films is modified to deconvolute the effects of the TCRs in the test column. The measured bulk thermal conductivity of

* Corresponding author. Tel.: +1 (778) 782 8538; fax: +1 (778) 782 7514.
E-mail addresses: mahadi@sfu.ca (M. Ahadi), mandishe@sfu.ca (M. Andisheh-Tadbir), Mickey.Tam@afcc-auto.com (M. Tam), mbahrami@sfu.ca (M. Bahrami).

http://dx.doi.org/10.1016/j.ijheatmasstransfer.2016.01.037
0017-9310/

Nomenclature

A	cross sectional area
a	overall radius of the double spiral disk
b	Y-intercept of line
D	a dimensionless function
h	thickness
I_0	modified Bessel function of the zeroth kind
j	counter variable
k	thermal conductivity
l	counter variable
m	slope of line
N	total number of measurement points
n	the number of concentric ring sources of the double spiral nickel
P	output power of the sensor
q	an arbitrary function
R	thermal resistance
R'	a combination of some bulk resistances and the thermal contact resistances in the TPS test column, $R' = \frac{h_{\text{Kap\&adh}}}{k_{\text{Kap\&adh}}A} + TCR$
$R_{\text{c,bm-s}}$	TCR between the background material and the sample
$R_{\text{b,s}}$	bulk thermal resistance of the sample
$R_{\text{c,s-Kap}}$	TCR between the sample and the Kapton layer
$R_{\text{b,Kap}}$	bulk thermal resistance of the Kapton layer
$R_{\text{c,Kap-adh}}$	TCR between the Kapton layer and the adhesive layer
$R_{\text{b,adh}}$	bulk thermal resistance of the adhesive layer
$R_{\text{b,Kap\&adh}}$	effective bulk thermal resistance of the Kapton layer and the adhesive layer together
$R_{\text{c,adh-p}}$	TCR between the adhesive layer and the nickel probe
r	total number of measurements
s	integration variable
s_b	the standard deviation of the intercept of the linear regression, $s_b = s_{y,x}\sqrt{\frac{1}{N} + \frac{x_{\text{ave}}^2}{SS_{xx}}}$
s_m	the standard deviation of the slope of the linear regression, $s_m = \frac{s_{y,x}}{\sqrt{SS_{xx}}}$
$s_{y,x}$	standard deviation of $y(x)$, $s_{y,x} = \sqrt{\frac{SS_E}{N-2}}$
SS_E	error sum of squares, $SS_E = \sum_{l=1}^{N}(y_l - \hat{y}_l)^2$
SS_{xx}	sum of squares, $SS_{xx} = \sum_{l=1}^{N}(x_l - x_{\text{ave}})^2$
SS_{xy}	sum of squares, $SS_{xy} = \sum_{l=1}^{N}(x_l - x_{\text{ave}})(y_l - y_{\text{ave}})$
T	temperature
t	time
TCR	thermal contact resistance
$T_{\gamma/2,N-2}$	the upper $100 \times \gamma/2\%$ point of the t-distribution with $N-2$ degrees of freedom
T_{I}	temperature of the surface of the background material facing the sensor
T_{II}	temperature of the nickel probe ($= \Delta T_{\text{p-bm}} + T_{\text{I}}$)
x	an arbitrary variable
y	an arbitrary variable
z	an arbitrary variable

Greek letters

α	temperature coefficient of resistivity of the probe
γ	significance level
Δ	difference operator
δ	uncertainty operator
Θ	characteristic time, $\Theta = a^2/\kappa_{\text{bm}}$
κ	thermal diffusivity
ρ	electrical resistance of the double spiral nickel
τ	dimensionless time, $\tau = \sqrt{t/\Theta}$

Subscripts

0	property at t=0 (s)
I	surface of the background material facing the sensor
II	surface of the nickel probe
adh	Adhesive sticking the Kapton layer to the nickel probe
app	apparent
ave	average
b	bulk property
bm	background material
c	contact
eff	effective property
f	thin film sample
i	initial
Kap	Kapton insulating layer
p	probe
s	sample
tot	total

Superscript

^	predicted by linear regression

ethylene tetrafluoroethylene (ETFE), Nafion, and gas diffusion layer (GDL) by the modified TPS method is presented and compared with the results of the guarded hot plate (GHP) method, as per ASTM Standard C177-13 [11].

2. Experimental methods

2.1. Existing TPS method for thin films

In this study, a hot disk TPS2500S Thermal Constants Analyser (Hot Disk AB, Gothenburg, Sweden and ThermTest Inc., Fredericton, Canada) is used. The TPS thin film sensor, shown in Fig. 1a, consists of a 10 μm thick double spiral nickel element, which is sandwiched between two 25 μm thick Kapton layers via some adhesive material [18]. According to the existing TPS method for thin films [18], the sensor is sandwiched between two equivalent pieces of a sample supported by a background material, as shown in Fig. 1b. In this study, two stainless steel blocks (SIS2343) were used as the background material, as shown in Fig. 2.

When the nickel element is heated, its temperature and, hence, its electrical resistance increases as a function of time, as follows [19]:

$$\rho(t) = \rho_0\{1 + \alpha\Delta T(t)\} = \rho_0\{1 + \alpha[\Delta T_{\text{p-bm}}(t) + \Delta T_{\text{ave,bm}}(t)]\} \quad (1)$$

where $\Delta T(t)$ is the probe mean temperature increase, $\Delta T_{\text{p-bm}}(t)$ is the temperature difference between the surfaces of the nickel probe and the background material, and $\Delta T_{\text{ave,bm}}(t)$ is the average temperature increase of the surface of the background material.$\Delta T_{\text{p-bm}}(t)$ becomes constant after a very short time, Δt_{i}, given by [19]:

$$\Delta t_{\text{i}} = \frac{h_{\text{p-bm}}^2}{\kappa_{\text{p-bm}}} \quad (2)$$

where $h_{\text{p-bm}}$ and $\kappa_{\text{p-bm}}$ are, respectively, the overall thickness and thermal diffusivity of the materials between the probe and the background material.

During a measurement, $\rho(t)$ is measured as a function of time [18], and the temperature increase of the probe is calculated from Eq. (1), as follows:

Table 1
Summary of capabilities and limitations of available transient measurement methods for thermal properties.

Technique	Capabilities and limitations	Standard
Hot wire	• Suitable for liquids, powders, non-carbonaceous materials, and dielectric materials • Not suitable for anisotropic materials • Applicable for $k < 15$ W·m^{-1}·K^{-1} • Temperature range from room temperature to 1500 °C • Long sensors and, consequently, long samples	ASTM C1113/C1113M-09 [12]
Hot strip	• Capable of measuring thermal conductivity, thermal diffusivity, and specific heat [14] • Suitable for solids and fluids with low electrical conductivity [14] • Long sensors and, consequently, long samples	Not available
Transient plane source (TPS)	• Capable of measuring thermal conductivity, thermal diffusivity, and specific heat • Suitable for solids, liquids, and powders • Suitable for both isotropic and anisotropic materials • Compact sensors and, consequently, small samples	ISO22007-2 [18]
Laser flash	• Suitable for homogenous, isotropic, and opaque solids • Diffusivity values from 0.1–1000 mm^2/s • Temperature range from 75–2800 K	ASTM E1461-13 [20]
3ω	• For measurement of thermal conductivity [21] • Suitable for dielectric solids [21] • Temperature range from 30 to 750 K [21]	Not available
Differential photoacoustic	• For measurement of thermal conductivity of thin films [23]	Not available
Pulsed photothermal displacement	• For measurement of thermal diffusivity of solids [24]	Not available
Thermal-wave	• For measurement of thermal diffusivity of high temperature superconductors [25] • Temperature range from 10 to 300 K [25]	Not available

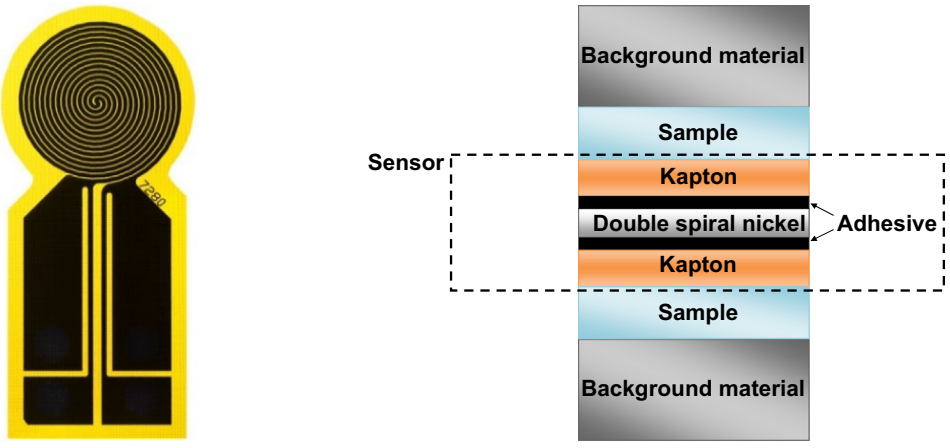

Fig. 1. (a) A picture of the TPS thin film sensor 7280, (b) schematic of the TPS test column.

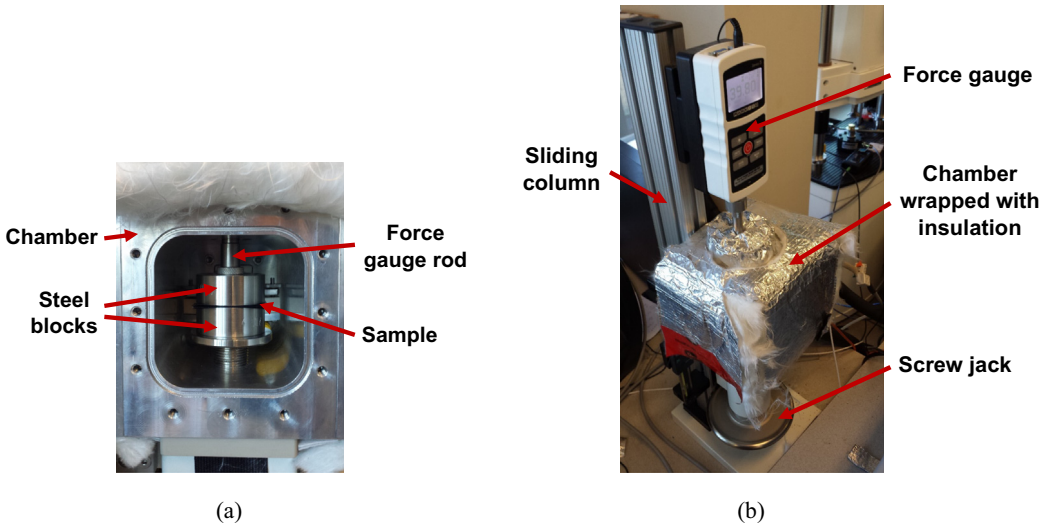

Fig. 2. (a) Inside of TPS2500S test chamber, (b) TPS test chamber and the applying force mechanism.

$$\Delta T(t) = \Delta T_{\text{p-bm}}(t) + \Delta T_{\text{ave,bm}}(t) = \frac{1}{\alpha}\left(\frac{\rho(t)}{\rho_0} - 1\right) \tag{3}$$

where $\Delta T_{\text{ave,bm}}$ is obtained from [19]:

$$\Delta T_{\text{ave,bm}}(\tau) = \frac{P_0}{\pi^{3/2} a k_{\text{bm}}} D(\tau) \tag{4}$$

where P_0 is the constant power of the sensor, and τ is a dimensionless time defined by [19]:

$$\tau = \sqrt{\frac{t}{\Theta}} \tag{5}$$

where Θ is a characteristic time defined by [19]:

$$\Theta = \frac{a^2}{\kappa_{\text{bm}}} \tag{6}$$

$D(\tau)$ in Eq. (4) is a dimensionless function, defined as [16,18]:

$$D(\tau) = \frac{1}{n^2(n+1)^2} \int_0^{\tau} \frac{1}{s^2} \left[\sum_{l=1}^{n} l \sum_{j=1}^{n} j \exp\left(-\frac{l^2 + j^2}{4n^2 s^2}\right) \times I_0\left(\frac{l \cdot j}{2n^2 s^2}\right) \right] ds \tag{7}$$

where I_0 is the modified Bessel function of the zeroth kind.

By substituting Eq. (4) into Eq. (3), the relation between $\Delta T(\tau)$ and $\Delta T_{\text{p-bm}}(\tau)$ becomes:

$$\Delta T(\tau) = \Delta T_{\text{p-bm}}(\tau) + \frac{P_0}{\pi^{3/2} a k_{\text{bm}}} D(\tau) \tag{8}$$

As $\Delta T_{\text{p-bm}}(\tau)$ becomes constant shortly after Δt_i and $\frac{P_0}{\pi^{3/2} a k_{\text{bm}}}$ is a constant for a specific experiment, Eq. (8) provides a linear relation between ΔT and $D(\tau)$ after Δt_i, whose slope and intercept are $\frac{P_0}{\pi^{3/2} a k_{\text{bm}}}$ and $\Delta T_{\text{p-bm}}$, respectively.

During an experiment, heat is imposed on the Kapton layer and the sample by the probe, which leads to increase in the temperature and, hence, electrical resistance of the probe. After obtaining the temperature increase of the heating element from Eq. (3), a value is guessed for κ_{bm}, and then, Θ in Eq. (6) and τ in Eq. (5) are calculated based on the guessed value. Then, $D(\tau)$ is calculated, and the curve of $\Delta T(\tau)$ versus $D(\tau)$ is plotted. If κ_{bm} was guessed correctly, the curve would be a line after a short dimensionless time $\Delta\tau_i$ associated with Δt_i, according to Eq. (8). Accordingly, the initial nonlinear section of the curve, associated with the initial transient conduction of heat across the Kapton layer and the sample, is discarded, and a linear regression is performed on the rest of the data which are registered during the steady state conduction of heat across the Kapton layer and the sample. Since τ is dependent on κ_{bm}, the linear regression analysis is performed on the data points iteratively. The above iterative process is shown in Fig. 3.

By using the obtained $\Delta T_{\text{p-bm}}$ from the final linear regression, the effective thermal conductivity of the materials between the nickel probe and the background material is calculated from [19]:

$$k_{\text{eff}} = \frac{P_0 h_{\text{p-bm}}}{2A\Delta T_{\text{p-bm}}} \tag{9}$$

As per ISO22007-2 [18], the following procedure is given for measuring the thermal conductivity of a thin film sample:

(1) A reference test with the thin film sensor alone between two slabs of the background material to determine the effective thermal conductivity of the Kapton layer together with the adhesive.
(2) An experiment with the sensor sandwiched between two identical pieces of the sample, supported by the slabs, to determine the effective thermal conductivity of the series combination of the adhesive layer, the Kapton layer, and the sample.

Then, according to ISO22007-2 [18], the effective thermal conductivity of the thin film (k_f) can be found from [18,26]:

$$R_{\text{tot}} = R_{\text{b,s}} + R_{\text{b,Kap\&adh}} \quad \text{or} \quad \frac{h_{\text{Kap\&adh}} + h_f}{k_{\text{eff}} A} = \frac{h_f}{k_f A} + \frac{h_{\text{Kap\&adh}}}{k_{\text{Kap\&adh}} A} \tag{10}$$

where $R_{\text{b,s}}$ is the bulk thermal resistance of the sample, and $R_{\text{b,Kap\&adh}}$ is the effective bulk thermal resistance of the Kapton layer and the adhesive.

2.2. The proposed modification for the existing TPS method for thin films and coatings

One important issue that has been acknowledged in the existing TPS thin film measurements [18] is the existence of a TCR between each of the two contacting surfaces in the TPS test column. As Bahrami et al. [27,28] also pointed out, at relatively low contact pressures, TCR between contacting surfaces can be much higher than the bulk resistance of a sample. Accordingly, deconvoluting the effects of the TCR in the TPS test column is of vital importance for obtaining accurate values of bulk thermal conductivity for thin films. The associated thermal resistance network of the TPS test

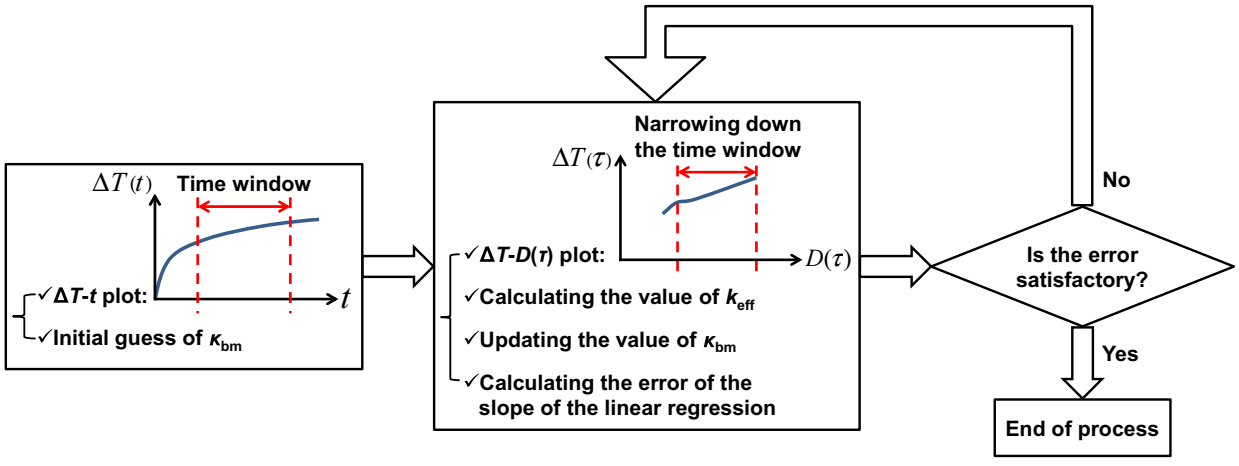

Fig. 3. Iterative process of TPS measurements.

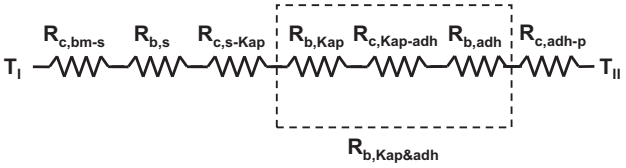

Fig. 4. Thermal resistance network of the TPS test column.

column, Fig. 1 b, is shown in Fig. 4. The definitions of the temperatures and thermal resistances in Fig. 4 are shown in the nomenclature. Therefore, instead of Eq. (10), the relationship between the thermal resistances in a TPS test column is:

$$\begin{aligned} R_{\text{tot}} &= R_{\text{c,bm-s}} + R_{\text{b,s}} + R_{\text{c,s-Kap}} + R_{\text{b,Kap\&adh}} + R_{\text{c,adh-p}} \\ &= R_{\text{c,bm-s}} + \frac{h_{\text{f}}}{k_{\text{f}}A} + R_{\text{c,s-Kap}} + \frac{h_{\text{Kap\&adh}}}{k_{\text{Kap\&adh}}A} + R_{\text{c,adh-p}} \\ &= \frac{h_{\text{f}}}{k_{\text{f}}A} + \frac{h_{\text{Kap\&adh}}}{k_{\text{Kap\&adh}}A} + TCR \end{aligned} \tag{11}$$

where $TCR = R_{\text{c,bm-s}} + R_{\text{c,s-Kap}} + R_{\text{c,adh-p}}$ is defined as the total contact resistance of the test column. In Eq. (11), the term $R_{\text{b,Kap\&adh}}$ takes the effect of $R_{\text{c,Kap-adh}}$ into account. By comparing Eqs. (10) and (11), it is clear that the effective thermal conductivity found for the sample by Eq. (10) is not the true bulk thermal conductivity of the sample and includes the effects of the TCRs of the TPS test column. In fact, it also includes the effect of TCR between the Kapton layer and the background material due to the performed reference tests, which may induce additional error in the measurements by the standard method because such a TCR does not exist in the measurement of the sample.

For convenience, Eq. (11) is rewritten as follows:

$$R_{\text{tot}} = \frac{h_{\text{f}}}{k_{\text{f}}A} + R' \tag{12}$$

where $R' = \frac{h_{\text{Kap\&adh}}}{k_{\text{Kap\&adh}}A} + TCR$.

The total thermal resistance in Eq. (12) should be back-calculated by substituting the values of h_{f}, k_{f}, $h_{\text{Kap\&adh}}$, and $k_{\text{Kap\&adh}}$ into Eq. (10). For more clarification, Eq. (10) is rewritten as follows, and the sequence of operations needed to back-calculate the total thermal resistance is also shown schematically in Fig. 5:

$$R_{\text{tot}} = \frac{(h_{\text{f}})_{\text{entered into the software}}}{(k_{\text{f}})_{\text{reported by the software}}A} + \frac{(h_{\text{Kap\&adh}})_{\text{entered into the software}}}{(k_{\text{Kap\&adh}})_{\text{entered into the software}}A} \tag{13}$$

After performing measurements for at least two thicknesses of a sample, the bulk thermal conductivity of the sample can be obtained by performing a linear regression on the obtained data of total resistance versus thickness. As shown in Eq. (12), the slope and intercept of such a line will yield the bulk thermal conductivity of the sample and the resistance, R', respectively. The developed method has the following advantages:

(1) Accurate measurement of the bulk thermal conductivity of thin films,

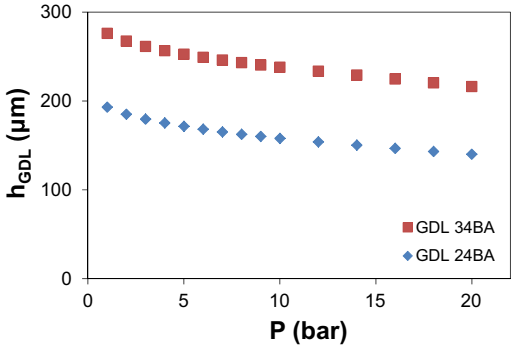

Fig. 6. Thicknesses of the GDL samples versus pressure measured by TUC_RUC.

(2) Elimination of the previously needed reference tests and the possibility of entering any values for h_{f}, $h_{\text{Kap\&adh}}$, and $k_{\text{Kap\&adh}}$ into the software due to the usage of the same values in back-calculation of the total resistance, and
(3) Elimination of the unwanted noise of the TCR between the Kapton layer and the background material induced by the standard reference tests.

The downside of the proposed method is the need for performing tests for at least two thicknesses of the same sample, which may not be available. In the next step, several case studies are performed on ETFE, Nafion, and GDL to investigate the proposed modified method. The thicknesses of the samples were measured by a custom-made testbed at Automotive Fuel Cell Cooperation Corp. (AFCC), known as the TUC_RUC machine, which has a sensitivity of 1 μm. The ETFE sheets were received from Asahi Glass Co. in thicknesses of 11, 24, 50, 105, and 204 μm, and the Nafion films were made in-house at AFCC in thicknesses of 10, 16, 26, and 48 μm. For GDL, two commercial samples with the names of GDL 24BA and GDL 34BA, received from SIGRACET®, are used. Fig. 6 shows thicknesses of the GDL samples versus pressure. Measurements are performed on the samples via the developed method and the GHP method described in Ref. [11], and the results of the two methods are compared and cross-checked against each other.

2.3. GHP method

The device for GHP measurements (ASTM Standard C177-13 [11]) is shown in Fig. 7. The details of the method and the device can be found elsewhere, see for example [4,11]. The total resistance of a sample measured by the GHP testbed is the summation of the sample bulk thermal resistance and the TCRs between the sample and the fluxmeters, as follows:

$$R_{\text{tot}} = \frac{h_{\text{f}}}{k_{\text{f}}A} + TCR \tag{14}$$

Therefore, similar to the modified TPS method, the thermal conductivity of the sample and the TCR of the test column should be obtained from a linear regression through the data of total resistance versus thickness of the sample.

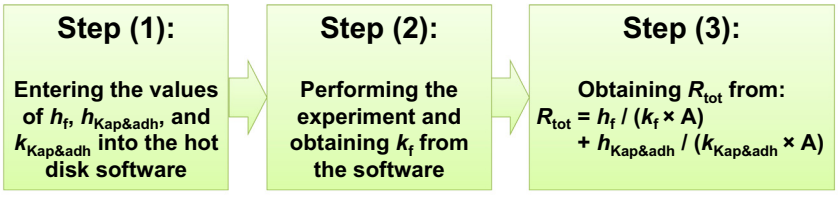

Fig. 5. Operations needed to back-calculate the total thermal resistance of a thin film from the hot disk software.

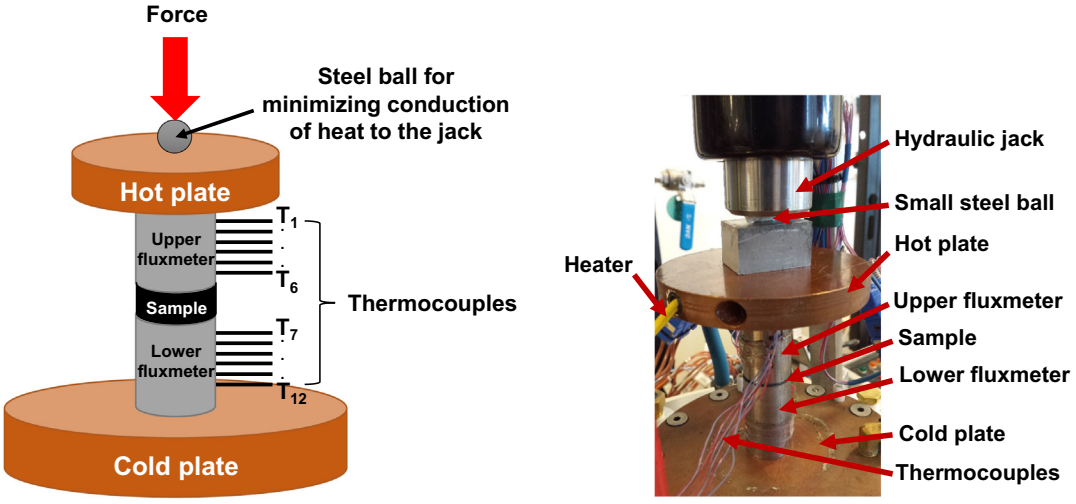

Fig. 7. (a) Schematic of the GHP testbed, (b) a picture of the GHP testbed with details.

3. Uncertainty analysis

The uncertainty analysis of the steady state and transient methods is performed following the methods described in Refs. [29,30], see Appendix A.

4. Results and discussion

To ensure an accurate measurement, lack of temperature drift for the nickel probe was ensured by allowing at least 5 min relaxation time prior to each measurement. Overall, each TPS measurement took ~3 min. For comparison, the first steady-state test by the GHP testbed took about 5 h, with subsequent tests at different pressures requiring ~2 h to reach steady-state condition.

4.1. ETFE results

In this study, for obtaining the raw data to incorporate in the developed method, values of 25 μm and 0.06 $W{\cdot}m^{-1}{\cdot}K^{-1}$ were arbitrarily chosen and entered into the hot disk software for the thickness and thermal conductivity of the Kapton film, respectively. To show that the value of Kapton thermal conductivity can be chosen arbitrarily in the developed method, a sensitivity analysis is performed. The conventional TPS thin film measurements [18] were also performed on the ETFE samples. The raw ETFE data obtained from the hot disk testbed are shown in Fig. 8. The values of k_{app}, shown in Fig. 8 and introduced in Eq. (13) by $(k_f)_{\text{reported by the software}}$, contain the effects of the TCRs of the TPS test column, which can be seen in the generally increasing trend of k_{app} with an increase in pressure. The TCRs decrease with an increase in pressure which leads to a higher k_{app}. In fact, the TCRs, inherent in the measurements, result in deviation from the actual thermal conductivity of ETFE; this issue will be discussed in more details later. For the 11 μm ETFE sample, the deviations are even larger due to the higher share of the TCRs compared to the film bulk resistance.

The data of different cases in Fig. 8 have been incorporated in the developed method to calculate the total thermal resistance values; the results are shown in Fig. 9 and show no noticeable changes in the measured total resistance by introduction of different values for the Kapton thermal conductivity into the software. The maximum uncertainty in the measured resistances is 1.3%.

To compare the TPS testbed with the GHP testbed, both results are plotted next to each other throughout the article. Since the TPS sensor and the GHP testbed fluxmeters have different cross sectional areas, the measured values of thermal resistance per unit area, i.e. thermal insulance [$K{\cdot}mm^2/W$], are compared.

Total thermal insulance versus thickness for ETFE is shown in Fig. 10. As shown, the linear behavior of total thermal insulance versus thickness is well captured by both methods. The maximum uncertainty for $R_{tot}A$ from 1 to 12 bar is 1.3% for the modified TPS

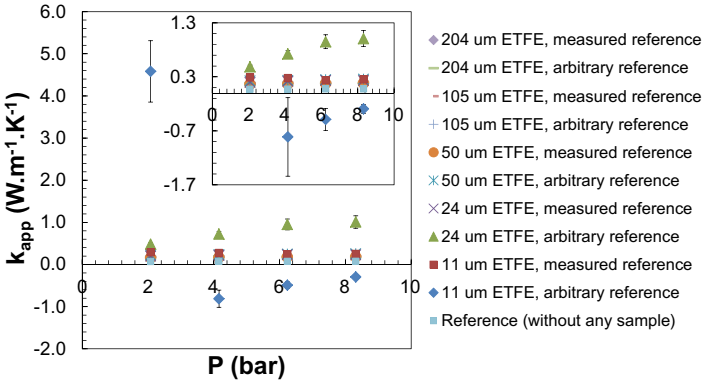

Fig. 8. The raw data obtained from the hot disk software for ETFE.

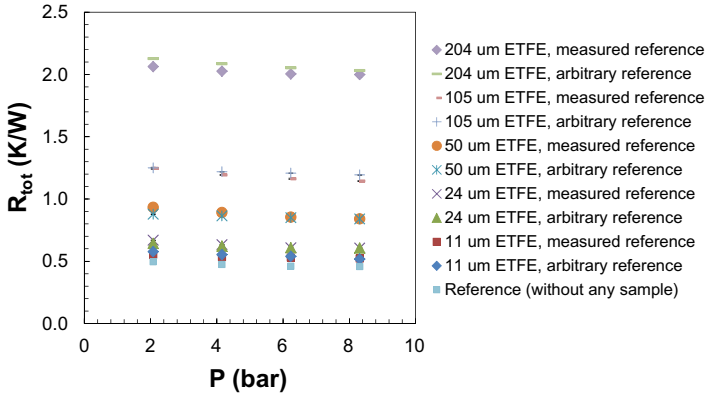

Fig. 9. Total thermal resistance versus pressure from the modified TPS method for ETFE.

method and 10.4% for the GHP method. As shown, the GHP testbed measures lower $R_{tot}A$ values than the TPS testbed, which is mainly due to the existence of the extra bulk resistance of the Kapton layer in the TPS test column compared to the GHP test column.

The changes in $R'A$ and $(TCR)A$ values versus pressure are plotted in Fig. 11. The decreasing trend of the data is due to the reduction of the TCRs in the test columns of the testbeds with increase in pressure. However, as can be inferred from the overlap of the uncertainty ranges of each data set, the total TCR for each data set does not change much with pressure, which is expected considering the almost flat surfaces of the ETFE films. The maximum uncertainties are 12.7% for $R'A$ and 32.5% for $(TCR)A$. The main reason for higher $R'A$ values than $(TCR)A$ values is the existence of the Kapton layer in the TPS test column. In addition, the fluxmeters of the GHP testbed have flat metallic surfaces, whereas the surfaces of the TPS sensor have some micro-patterns; this can result in higher contact insulances in the TPS test column than the GHP test column.

The measured thermal conductivities at different pressures are shown in Fig. 12 next to the results of the conventional TPS thin film theory. The results of the modified TPS method in Fig. 12 show how well the raw data of the hot disk testbed shown in Fig. 8 collapse onto a consistent value of thermal conductivity when incorporated in the developed method. Fig. 12 also shows a consistent measurement of thermal conductivity of ETFE by the modified TPS method and the GHP method. In addition, comparing the obtained consistent thermal conductivity values from the modified TPS method with the values from the conventional TPS method

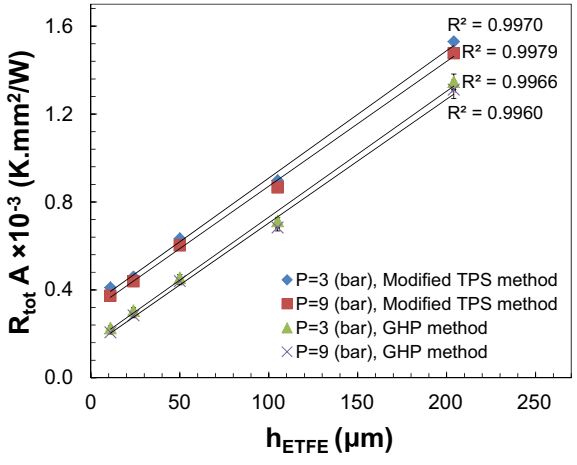

Fig. 10. Total thermal insulance versus thickness for ETFE.

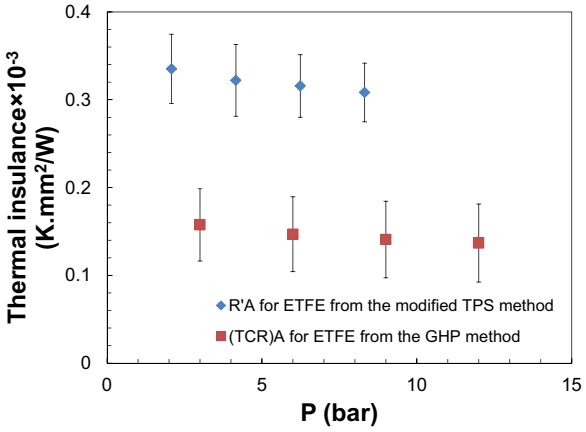

Fig. 11. $R'A$ from the modified TPS method next to $(TCR)A$ from the GHP method for ETFE.

further uncovers the significant effects of TCR in the results of the conventional method, up to 66.7% relative difference. As shown in Fig. 12, the TCR effects decrease as the thickness of ETFE increases, the reason of which is decrease in the share of the TCRs in the total resistance with an increase in the thickness of ETFE. The maximum uncertainties in Fig. 12 are 6.7% for the proposed modified TPS method and 7.5% for the GHP method. The average value of thermal conductivity of ETFE is 0.174 ± 0.002 W·m^{-1}·K^{-1} from the modified TPS method and 0.177 ± 0.002 W·m^{-1}·K^{-1} from the GHP method.

4.2. Nafion results

The Results of Nafion are shown through Figs. 13–15. Similar to Fig. 10, both methods well capture the linear trend of the total insulance versus thickness. Fig. 14 shows lower $(TCR)A$ values for Nafion compared to that of ETFE shown in Fig. 11, which could be due to the softer and more deformable nature of Nafion membranes leading to the membranes to conform more to the flat metallic surfaces of the fluxmeters of the GHP testbed. In comparison with ETFE, the change in $R'A$ with pressure is significant for Nafion. The relative difference between the thermal conductivity results of the two methods, shown in Fig. 15, is about 13.5%. The average thermal conductivity of Nafion measured by the modified TPS method is 0.243 ± 0.007 W·m^{-1}·K^{-1}, whereas the average value measured by the GHP method is 0.214 ± 0.003 W·m^{-1}·K^{-1}. Since the share of bulk resistance of Nafion in total resistance is larger in the GHP method, the thermal conductivity results of this

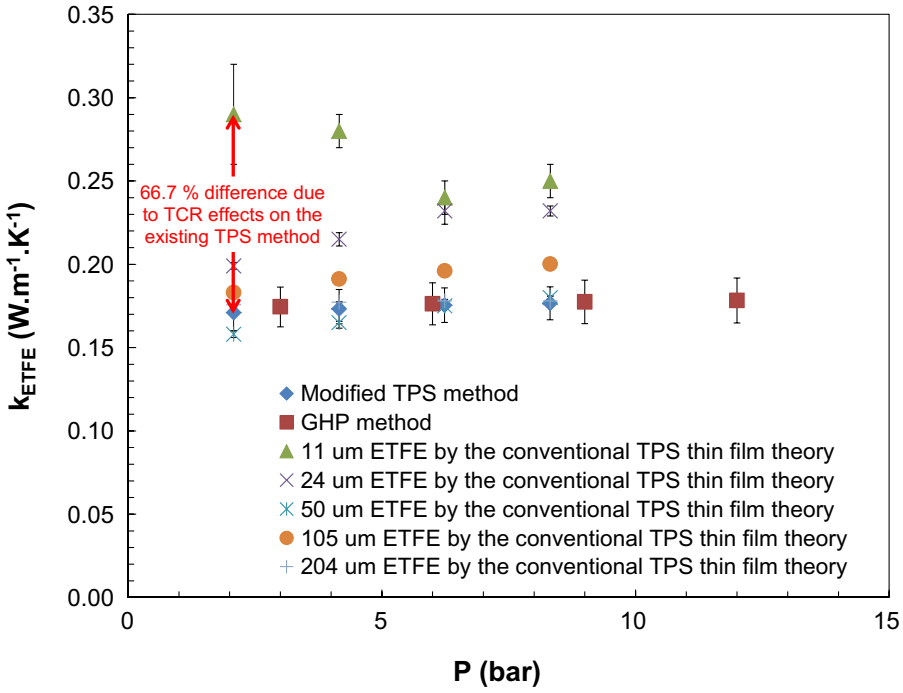

Fig. 12. Thermal conductivity of ETFE versus pressure.

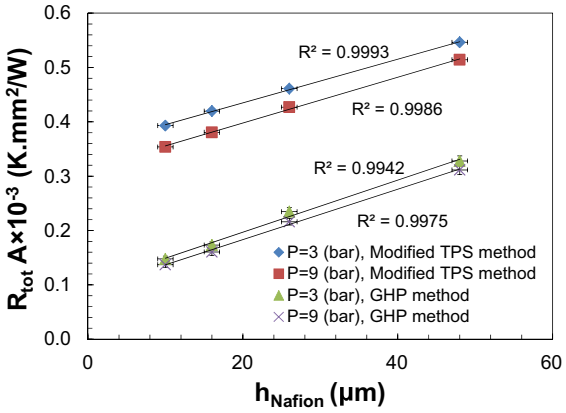

Fig. 13. Total thermal insulance versus thickness for Nafion.

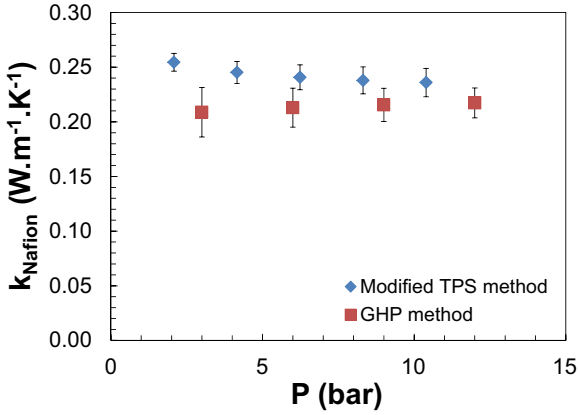

Fig. 15. Thermal conductivity of Nafion versus pressure.

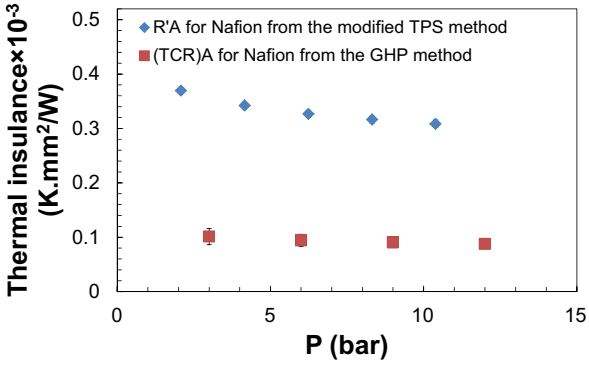

Fig. 14. $R'A$ from the modified TPS method next to $(TCR)A$ from the GHP method for Nafion.

method for Nafion are more accurate than the values obtained by the modified TPS method.

4.3. GDL results

For GDL, two samples, namely GDL 24BA and GDL 34BA, are measured. The GDL results are shown in Figs. 16–18. Fig. 16 shows the decreasing trend of total insulance versus compressive load. Fig. 17, again, shows higher $R'A$ values than $(TCR)A$ values for GDL. Since the zero insulance is generally in the uncertainty ranges of the negative values in Fig. 17, these values can be interpreted as small positive insulances which are close to zero. As shown in Fig. 18, thermal conductivity of GDL increases with an increase in pressure. The reason for this behavior is given in several studies in literature [4,31,32].

The thermal conductivity values of GDL measured by the two methods are about 15.7% different from each other which could

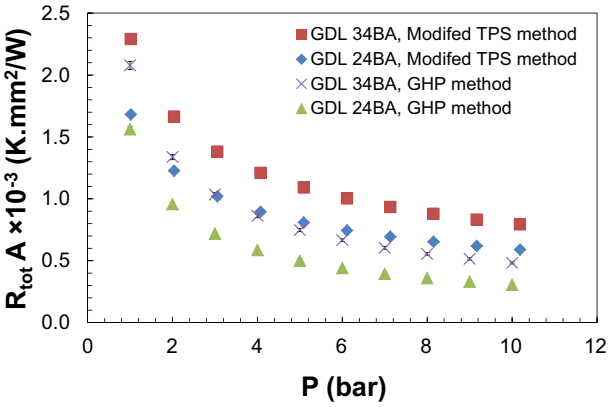

Fig. 16. Total insulance of GDL from the modified TPS method and the GHP method.

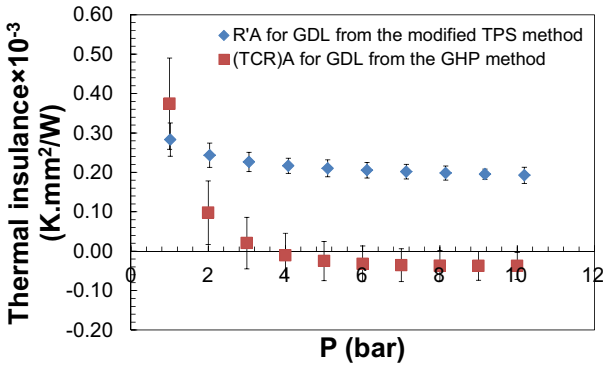

Fig. 17. *R′A* from the modified TPS method next to *(TCR)A* from the GHP method for GDL.

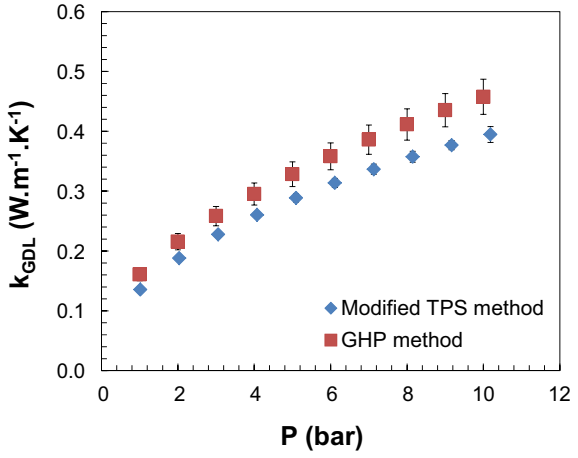

Fig. 18. Thermal conductivity of GDL versus pressure.

mainly be attributed to hysteresis behavior of GDL materials under compressive load due to their fibrous porous structure as explained in details in Ref. [31]. In the GHP testbed, the fluxmeters undergo a series of thermal expansions and contractions until the device reaches the steady state, whereas in the TPS testbed, these effects are not present, as it is a transient and fast test. Accordingly, GDL experiences some hysteresis effects in the GHP testbed at each stage of pressure increment, whereas the TPS results for GDL are free of such effects. The maximum uncertainties in the obtained values of GDL thermal conductivity are 3.4% for the results of the modified TPS method and 6.6% for the results of the GHP method.

Overall, when selecting a measurement method for measuring thermal conductivity of a thin film or coating, the mechanical behavior of the sample should be taken into consideration. However, considering the much longer time required for GHP measurements compared to modified TPS tests, one can conclude that the proposed method is a valuable and efficient tool for accurate measurement of thermal conductivity of thin films and coatings.

5. Conclusions

In this study, the conventional TPS thin film theory was modified by deconvoluting the effects of TCRs in the TPS test column. The proposed modification can also eliminate the need for conducting any reference tests required by the conventional method. Instead, one should conduct measurements on at least two thicknesses of the same sample. To validate the developed method, ETFE sheets, Nafion films, and GDL samples were tested by both the developed method and the GHP method. The results of the two methods are summarized in Table 2. It was explained that the differences between the results of the two methods originated from different mechanical behaviors of a sample in the testbeds and show the importance of considering such features while selecting the thermal conductivity measurement method.

Acknowledgements

The authors gratefully acknowledge the financial support received from the Natural Sciences and Engineering Research Council of Canada (NSERC) through NSERC Collaborative Research Development Grant No. 31-614105, Ms. Keping Wang from Automotive Fuel Cell Cooperation Corp. (AFCC) for making the thin Nafion films, and Asahi Glass Co. for providing free ETFE samples.

Appendix A

According to [29], if q is any function of several variables $x, \ldots, z$, then the uncertainty in q is calculated by:

$$\delta q = \sqrt{\left(\frac{\partial q}{\partial x}\delta x\right)^2 + \ldots + \left(\frac{\partial q}{\partial z}\delta z\right)^2} \tag{A1}$$

According to [30], if a linear regression $\hat{y} = \hat{m}x + \hat{b}$ is performed on the set of ordered pairs (x, y), the uncertainties of the slope and intercept of the regression should be found from:

Table 2
Summary of the thermal conductivity results.

Sample	Measurement method	k (W·m^{-1}·K^{-1})	Uncertainty (%)	Relative difference (%)
ETFE	Modified TPS	0.174 ± 0.002	1.1	1.7
	GHP	0.177 ± 0.002	1.1	
Nafion	Modified TPS	0.243 ± 0.007	2.9	13.5
	GHP	0.214 ± 0.003	1.4	
GDL (1 to 10 bar)	Modified TPS	0.135 – 0.395	3.4	15.7
	GHP	0.16 – 0.46	6.6	

$$\delta\hat{m} = T_{\gamma/2,N-2}s_m \tag{A2}$$

$$\delta\hat{b} = T_{\gamma/2,N-2}s_b \tag{A3}$$

where $T_{\gamma/2,N-2}$ is the upper $100\times\gamma/2\%$ point of the t-distribution with $N-2$ degrees of freedom; γ is the significance level for which the value 0.05 is mostly used; N is the total number of measurement points, and s_m and s_b are the standard deviations of the slope and the intercept of the fitted line, respectively. Moreover, s_m and s_b are calculated from the following equations:

$$s_m = \frac{s_{y,x}}{\sqrt{SS_{xx}}} \tag{A4}$$

$$s_b = s_{y,x}\sqrt{\frac{1}{N}+\frac{x_{\text{ave}}^2}{SS_{xx}}} \tag{A5}$$

$$SS_{xx} = \sum_{l=1}^{N}(x_l - x_{\text{ave}})^2 \tag{A6}$$

$$x_{\text{ave}} = \frac{1}{N}\sum_{l=1}^{N}x_l \tag{A7}$$

$$s_{y,x} = \sqrt{\frac{SS_E}{N-2}} \tag{A8}$$

$$SS_E = \sum_{l=1}^{N}(y_l - \hat{y}_l)^2 \tag{A9}$$

$$\hat{y}_l = \hat{m}x_l + \hat{b} \tag{A10}$$

$$\hat{m} = \frac{SS_{xy}}{SS_{xx}} \tag{A11}$$

$$SS_{xy} = \sum_{l=1}^{N}(x_l - x_{\text{ave}})(y_l - y_{\text{ave}}) \tag{A12}$$

$$y_{\text{ave}} = \frac{1}{N}\sum_{l=1}^{N}y_l \tag{A13}$$

$$\hat{b} = y_{\text{ave}} - \hat{m}x_{\text{ave}} \tag{A14}$$

If several values of quantity q are measured and the average of the measurements is reported as the final value, then, the standard deviation of the reported average is obtained from:

$$\text{Standard deviation of } q = \sqrt{\frac{\sum_{l=1}^{r}(q_l - q_{\text{ave}})^2}{r}} \tag{A15}$$

where r is the total number of measurements and $q_{\text{ave}} = \frac{1}{r}\sum_{l=1}^{r}q_l$.

References

[1] N. Zamel, E. Litovsky, S. Shakhshir, X. Li, J. Kleiman, Measurement of in-plane thermal conductivity of carbon paper diffusion media in the temperature range of −20 °C to +120 °C, Appl. Energy 88 (9) (2011) 3042–3050.

[2] G. Karimi, X. Li, P. Teertstra, Measurement of through-plane effective thermal conductivity and contact resistance in PEM fuel cell diffusion media, Electrochim. Acta 55 (5) (2010) 1619–1625.

[3] S.G. Kandlikar, Z. Lu, Thermal management issues in a PEMFC stack-a brief review of current status, Appl. Therm. Eng. 29 (7) (2009) 1276–1280.

[4] E. Sadeghi, N. Djilali, M. Bahrami, Effective thermal conductivity and thermal contact resistance of gas diffusion layers in proton exchange membrane fuel cells. Part 1: effect of compressive load, J. Power Sources 196 (1) (2011) 246–254.

[5] O.S. Burheim, H. Su, H.H. Hauge, S. Pasupathi, B.G. Pollet, Study of thermal conductivity of PEM fuel cell catalyst layers, Int. J. Hydrogen Energy 39 (17) (2014) 9397–9408.

[6] B. Abeles, Lattice thermal conductivity of disordered semiconductor alloys at high temperatures, Phys. Rev. Lett. 131 (1963) 1906–1911.

[7] R.J. McGlen, R. Jachuck, S. Lin, Integrated thermal management techniques for high power electronic devices, Appl. Therm. Eng. 24 (8–9) (2004) 1143–1156.

[8] S.V. Garimella, T. Persoons, J. Weibel, L.T. Yeh, Technological drivers in data centers and telecom systems: multiscale thermal, electrical, and energy management, Appl. Energy 107 (2013) 66–80.

[9] L.L. Kerr, Y.L. Pan, R.B. Dinwiddie, H. Wang, R.C. Peterson, Thermal conductivity of coated paper, Int. J. Thermophys. 30 (2) (2009) 572–579.

[10] R.F. Speyer, Thermal Analysis of Materials, Marcel Dekker, New York, 1994.

[11] ASTM C177-13, Standard test method for steady-state heat flux measurements and thermal transmission properties by means of the guarded-hot-plate apparatus, ASTM International, West Conshohocken, PA, 2013, <www.astm.org>.

[12] ASTM C1113/C1113M-09 (2013), Standard test method for thermal conductivity of refractories by hot wire (platinum resistance thermometer technique), ASTM International, West Conshohocken, PA, 2013, <www.astm.org>.

[13] S.E. Gustafsson, A non-steady-state method of measuring the thermal conductivity of transparent liquids, Z. Naturforsch. Sec. A–A J. Phys. Sci. 22 (7) (1967) 1005–1011.

[14] S.E. Gustafsson, E. Karawacki, M.N. Khan, Transient hot-strip method for simultaneously measuring thermal conductivity and thermal diffusivity of solids and fluids, J. Phys. D-Appl. Phys. 12 (9) (1979) 1411–1421.

[15] S.E. Gustafsson, E. Karawacki, M.A. Chohan, Thermal transport studies of electrically conducting materials using the transient hot-strip technique, J. Phys. D-Appl. Phys. 19 (5) (1986) 727–735.

[16] S.E. Gustafsson, Transient plane source techniques for thermal conductivity and thermal diffusivity measurements of solid materials, Rev. Sci. Instrum. 62 (3) (1991) 797–804.

[17] M. Gustavsson, E. Karawacki, S.E. Gustafsson, Thermal conductivity, thermal diffusivity, and specific heat of thin samples from transient measurements with hot disk sensors, Rev. Sci. Instrum. 65 (12) (1994) 3856–3859.

[18] ISO22007-2, Plastics-determination of thermal conductivity and thermal diffusivity-part 2: transient plane heat source (hot disc) method, 2008, pp. 1–16.

[19] J.S. Gustavsson, M. Gustavsson, S.E. Gustafsson, On the use of the hot disk thermal constants analyser for measuring the thermal conductivity of thin samples of electrically insulating materials, in: Proceedings of the 24th International Thermal Conductivity Conference, Technomic Publishing Company Inc, Lancaster, PA, 1999, pp. 116–122.

[20] ASTM E1461-13, Standard test method for thermal diffusivity by the flash method, ASTM International, West Conshohocken, PA, 2013, <www.astm.org>.

[21] D.G. Cahill, Thermal conductivity measurement from 30 to 750 K: the 3ω method, Rev. Sci. Instrum. 61 (2) (1990) 802–808.

[22] D.G. Cahill, M. Katiyar, J.R. Abelson, Thermal conductivity of a-Si:H thin films, Phys. Rev. B 50 (9) (1994) 6077–6081.

[23] S. Govorkov, W. Ruderman, M.W. Horn, R.B. Goodman, M. Rothschild, A new method for measuring thermal conductivity of thin films, Rev. Sci. Instrum. 68 (10) (1997) 3828–3834.

[24] G.L. Bennis, R. Vyas, R. Gupta, S. Ang, W.D. Brown, Thermal diffusivity measurement of solid materials by the pulsed photothermal displacement technique, J. Appl. Phys. 84 (7) (1998) 3602–3610.

[25] V. Calzona, M.R. Cimberle, C. Ferdeghini, M. Putti, A.S. Siri, Fully automated apparatus for thermal diffusivity measurements on HTSC in high magnetic field, Rev. Sci. Instrum. 64 (3) (1993) 766–773.

[26] H. Zhang, M.J. Li, W.Z. Fang, D. Dan, Z.Y. Li, W.Q. Tao, A numerical study on the theoretical accuracy of film thermal conductivity using transient plane source method, Appl. Therm. Eng. 72 (1) (2014) 62–69.

[27] M. Bahrami, M.M. Yovanovich, J.R. Culham, Thermal joint resistances of conforming rough surfaces with gas-filled gaps, J. Thermophys. Heat Transfer 18 (3) (2004) 318–325.

[28] M. Bahrami, J.R. Culham, M.M. Yovanovich, Modeling thermal contact resistance: a scale analysis approach, J. Heat Transfer-Trans. ASME 126 (6) (2004) 896–905.

[29] J.R. Taylor, An introduction to error analysis: the study of uncertainties in physical measurements, Second ed., University Science Books, Sausalito, 1982.

[30] D.C. Montgomery, G.C. Runger, Applied statistics and probability for engineers, Third ed., John Wiley & Sons Inc, New York, 2003.

[31] E. Sadeghi, N. Djilali, M. Bahrami, Effective thermal conductivity and thermal contact resistance of gas diffusion layers in proton exchange membrane fuel cells. Part 2: hysteresis effect under cyclic compressive load, J. Power Sources 195 (24) (2010) 8104–8109.

[32] E. Sadeghi, M. Bahrami, N. Djilali, Analytic determination of the effective thermal conductivity of PEM fuel cell gas diffusion layers, J. Power Sources 179 (1) (2008) 200–208.